ANNUAL REVIEWS

Annual Review of Vision Science

Spike–Gamma Phase Relationship in the Visual Cortex

Supratim Ray

Centre for Neuroscience, Indian Institute of Science, Bangalore, India 560012;
email: sray@iisc.ac.in

Annu. Rev. Vis. Sci. 2022. 8:361–81

First published as a Review in Advance on June 6, 2022

The *Annual Review of Vision Science* is online at vision.annualreviews.org

https://doi.org/10.1146/annurev-vision-100419-104530

Keywords

gamma, visual cortex, local field potential, LFP, phase, oscillations

Abstract

Gamma oscillations (30–70 Hz) have been hypothesized to play a role in cortical function. Most of the proposed mechanisms involve rhythmic modulation of neuronal excitability at gamma frequencies, leading to modulation of spike timing relative to the rhythm. I first show that the gamma band could be more privileged than other frequencies in observing spike–field interactions even in the absence of genuine gamma rhythmicity and discuss several biases in spike–gamma phase estimation. I then discuss the expected spike–gamma phase according to several hypotheses. Inconsistent with the phase-coding hypothesis (but not with others), the spike–gamma phase does not change with changes in stimulus intensity or attentional state, with spikes preferentially occurring 2–4 ms before the trough, but with substantial variability. However, this phase relationship is expected even when gamma is a byproduct of excitatory–inhibitory interactions. Given that gamma occurs in short bursts, I argue that the debate over the role of gamma is a matter of semantics.

INTRODUCTION

Brain signals often show rhythmic fluctuations between 30 and 70 Hz, called gamma oscillations, which are modulated by cognitive processes such as attention (Fries et al. 2001) and have been hypothesized to play a fundamental role in cortical processing (Fries 2009). In the visual cortex, the focus of this review, both the magnitude and the center frequency of these oscillations are highly dependent on features of the visual stimulus such as size, contrast, orientation, spatial frequency, speed, eccentricity, and color (Bartoli et al. 2019; Berens et al. 2008; Friedman-Hill et al. 2000; Gieselmann & Thiele 2008; Hadjipapas et al. 2007; Jia et al. 2013b; Murty et al. 2018; Ray & Maunsell 2010, 2011a; Shirhatti & Ray 2018; van Pelt & Fries 2013). I and others have previously suggested that such a strong dependence on low-level stimulus features, as well as the weak and inconsistent power of gamma rhythm, makes gamma unsuitable for communication or coding; instead, it could be a useful reflection of underlying cortical processing involving excitation–inhibition interactions (Bartoli et al. 2020, Ray & Maunsell 2015).

Gamma oscillations are thought to arise due to the involvement of an inhibitory network that provides rhythmic inhibition to the pyramidal cells (Bartos et al. 2007, Buzsáki & Wang 2012, Whittington et al. 2000). Most of the hypothesized roles of gamma involve a shift in the timing of action potentials relative to this rhythm (Fries 2015, Fries et al. 2007, Tiesinga & Sejnowski 2010). This rhythmic modulation in neuronal excitability can be well characterized in the local field potential (LFP), which is obtained by low-pass filtering of the raw signal recorded from a microelectrode and is thought to reflect the summed transmembrane currents flowing through the neurons around the microelectrode (Buzsáki et al. 2012, Einevoll et al. 2013). Spike–LFP phase relationships are characterized by two factors: the preferred LFP phase at which spikes occur and the consistency with which spikes occur at that phase. These are typically estimated using measures such as spike–field coherency (SFC) (Mitra & Pesaran 1999), a complex quantity whose phase gives the preferred LFP phase and whose magnitude, termed coherence, gives a measure of phase consistency. Unfortunately, SFC is biased by several factors (discussed below), which complicates its interpretation. In this review, I discuss some of these issues, focusing especially on cases where the gamma observed in the LFP is weak or negligible, and then review the expected and observed spike–LFP phase relationships under various hypotheses.

SPIKE–FIELD COHERENCE IN THE ABSENCE OF GAMMA RHYTHM

Accurate estimation of the LFP gamma phase relative to a spike is fraught with difficulties (Ray 2015). Spikes are associated with several stereotypical fluctuations in the LFP, most prominently a sharp transient that is well represented by a negative Gaussian with a standard deviation of a few milliseconds (Martin & Schröder 2016, Rasch et al. 2008, Ray & Maunsell 2011b, Ray et al. 2008; for examples, see Ray 2015, figure 2). This spike-related transient, which may occur due to fast synaptic events that lead to the spike (Okun et al. 2010) and the low-frequency component of the spike itself (bleed-through), has energy over a broad frequency range, which can be detected in the LFP at frequencies as low as approximately 50 Hz [at lower frequencies, it gets masked by the 1/f power of the LFP (Ray 2015, Ray & Maunsell 2011a, Ray et al. 2008)]. This spike-related transient affects the gamma phase and can also cause spurious bumps in the gamma range in the SFC, as illustrated below.

Some studies have shown an absence of a conspicuous peak in the power spectral density (PSD) of the LFP but a peak in SFC in the gamma range, which has been taken as evidence of spike–gamma synchronization even when the rhythm is not detected as a peak in the PSD (for example, the prestimulus period; see Fries et al. 2008, Vinck et al. 2013). This is illustrated in a recent study (Prakash et al. 2021; **Figure 1**). In this case, spikes and LFPs were recorded from

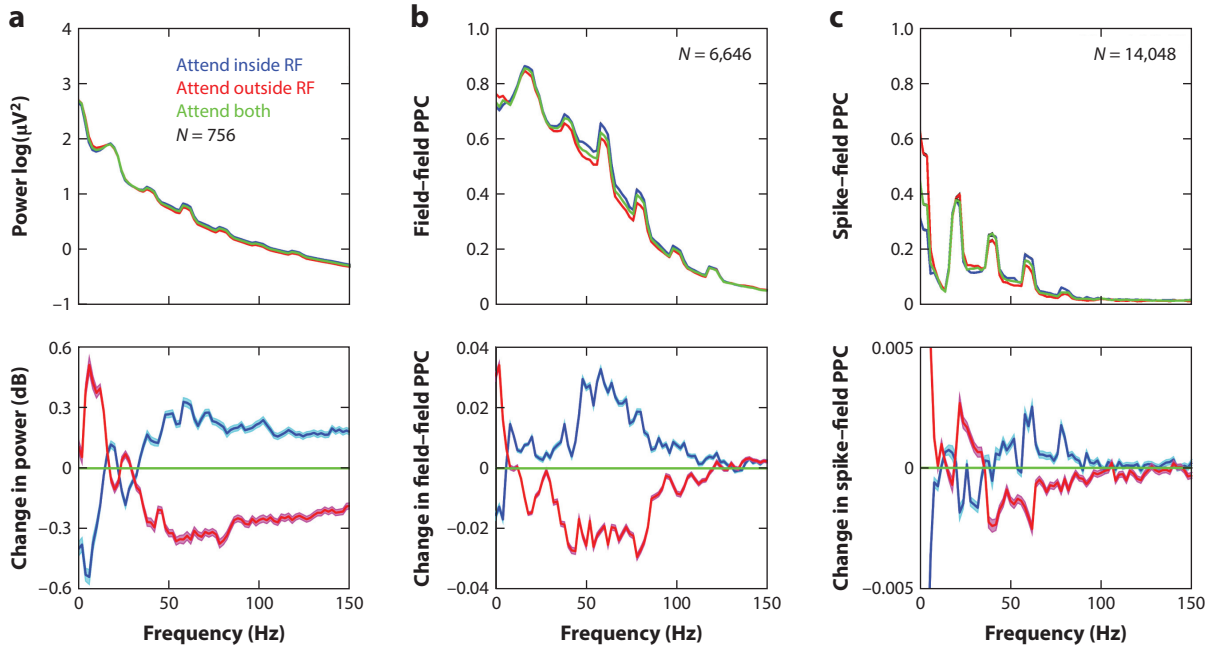

Figure 1

Coherence measures often show a bump in the gamma range even when the power spectral density (PSD) does not. (*a*) (*Top*) Average PSD of 756 electrodes recorded from area V4 across 25 sessions from two monkeys using Utah arrays while two stimuli counterphasing at 10 Hz were presented. The monkeys attended to the stimulus either inside (*blue*) or outside (*red*) the receptive fields (RFs). In a separate block of trials, the monkeys were cued to both sides (neutral cue; *green*). The counterphasing stimulus produced salient peaks at 20 Hz and harmonics. (*Bottom*) The change in power in the local field potential (LFP) from the neutral condition. Since the PSDs are plotted on a log scale in the top panel, the change is computed by simply subtracting the green trace from others and multiplying by 10 to get units of decibels. The cyan and magenta shades around the blue and red traces represent standard error of the mean. (*b*) (*Top*) Average field–field pairwise phase consistency (PPC) across 6,646 pairs of electrodes for the three attention conditions. (*Bottom*) The difference from the neutral condition, as in panel *a* (*bottom*). (*c*) Spike–field coherence between 14,048 pairs of spike and LFP electrodes, with the same format as in panel *b*. Figure adapted from Prakash et al. (2021).

both hemispheres of area V4 of rhesus monkeys who were shown two Gabor stimuli in opposite hemifields that were counterphasing at 10 Hz. Each stimulus was placed inside the receptive fields (RFs) of recorded neurons in each hemisphere. The monkeys were instructed to attend to either one of the two stimuli or both stimuli simultaneously (neutral condition) (for details of task design, see Mayo & Maunsell 2016). Such counterphasing stimuli produce salient sharp peaks in the PSDs at twice the fundamental frequency (i.e., at 20 Hz and its harmonics), since luminance change in either the positive or negative direction produces a response. Such peaks were observed for all three attention conditions, but no other peak in the gamma range was observed (**Figure 1*a***). However, a suppression of power at low frequencies (<20 Hz) and an enhancement over a broad frequency range above 30 Hz (with a shallow peak in the gamma range) could be observed with attention when the change in power was computed relative to the neutral condition (**Figure 1*a***). To measure phase consistency in the LFPs across electrode pairs, pairwise phase consistency (PPC), an unbiased estimator of the square of the SFC, was used (Vinck et al. 2010b, 2012). **Figure 1*b*** shows the field–field (LFP–LFP) PPC across all pairs of selected electrodes and the difference in PPC from the neutral condition. In this case, the effect of attention is more prominent in the gamma range as compared to change in power, as shown in **Figure 1*a***.

Spike–field PPC (**Figure 1*c***) showed that spikes were tightly locked to the fundamental and harmonics of the counterphasing stimulus. However, when the neutral condition was subtracted (**Figure 1*c***), the effect of attention appeared most saliently in the gamma range. Such results have previously been used to suggest that spike–gamma synchronization can occur even when the rhythm itself is not detectable in the PSD of the LFP (prestimulus period; see Fries et al. 2008).

The following simulation shows how such an effect could arise in the absence of any genuine gamma synchronization simply because the SFC itself is insensitive at high frequencies due to small jitters in spikes across electrodes (as explained below) and at low frequencies due to high LFP power that is unrelated to spiking. I compute the SFC between spikes from one electrode and the LFP from a neighboring electrode that is sufficiently far away that the same spike is not recorded in the neighboring electrode. This is a common approach that is thought to eliminate the effect of the spike-related transient. However, spiking activity is correlated across electrodes over several millimeters (Smith & Kohn 2008), which means that when a spike is detected on one electrode, there is a higher-than-chance probability of spiking (from a different neuron) in the neighboring electrode as well. Furthermore, spikes on each electrode are associated with their own spike-related transient that is captured in the LFP of that electrode.

Consider a hypothetical case where each spike is associated with a sharp negative Gaussian in the LFP, and the LFP has no other contribution from any other source. Furthermore, suppose that spikes produced by two different neurons near to the two recording electrodes occur in perfect synchrony. In this case, the simulated LFP of a neighboring electrode (which will be the same as the LFP recorded from the spike electrode itself) will show a negative Gaussian for each spike (**Figure 2*a***). Such sharp transients lead to energy over a large frequency range (**Figure 2*b***) and can be approximated as a sum of a series of sinusoids with their troughs aligned. The spike-triggered average of the LFP, obtained by taking short segments of LFP around each spike and averaging them, yields the original negative Gaussian (**Figure 2*c***). Since this phase relationship is consistent across trials at all frequencies, the SFC is almost unity at all frequencies (**Figure 2*d***).

Now consider a case where the two neurons fire spikes with a jitter of varying magnitudes. This could happen due to the stochasticity associated with firing that leads to a cross-correlation with a broadish peak (Smith & Kohn 2008). This jitter shifts the position of the negative Gaussian relative to each spike (the jitter of up to ± 5 ms is shown in **Figure 2*a***). However, this absolute time shift corresponds to a progressively larger phase shift for higher-frequency components of the negative Gaussian, which leads to a smoothing of the spike-triggered LFP average (**Figure 2*c***) and a reduction in the SFC at progressively higher frequencies (**Figure 2*d***). This produces a natural low-pass effect.

Figure 2*e–b* shows the same analysis as **Figure 2*a–d***, but after adding the real LFP signal recorded during periods of spontaneous activity to the simulated negative Gaussians. Because the LFP has a characteristic 1/f power law (**Figure 2*f***), the low-frequency component of the LFP that is unrelated to the spiking activity (Mitzdorf 1985) masks out the component due to the spike-related transient at low frequencies, reducing the SFC at low frequencies. This produces a natural high-pass effect. Together, these two factors combine to yield a band-pass effect, which produces a distinct bump in the gamma range in the SFC (**Figure 2*b***), even though there is no genuine gamma rhythm in the LFP.

The SFC is also biased by factors such as firing rates and number of trials, and several methods have been developed to address some of these concerns (Grasse & Moxon 2010; Li et al. 2016; Lowet et al. 2016; Ray 2015; Ray & Maunsell 2015; Vinck et al. 2010b, 2012). The issue discussed above, however, is not a mathematical but a physiological one. As described above, the effect of the spike-related transient is reduced, but not completely eliminated, by recording the LFP from a nearby electrode, since spiking activity remains correlated over several millimeters (Smith & Kohn

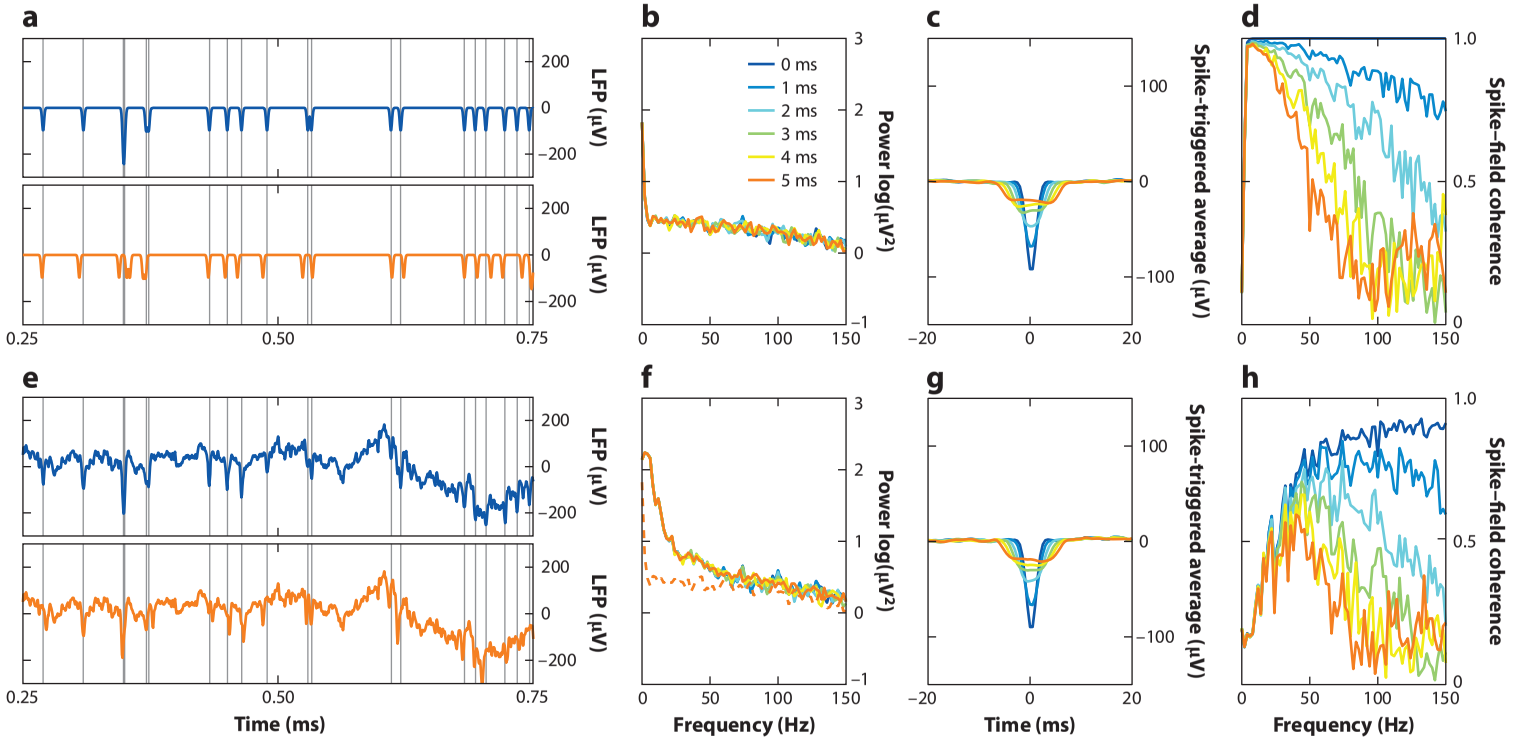

Figure 2

Factors leading to a bump in spike–field coherence in the gamma range in the absence of a genuine gamma rhythm. (*a*) Simulations of 50 trials of Poisson-distributed spike trains with a mean firing rate of 40 Hz and duration of 1 s. Spike times for one trial are shown by gray vertical lines. (*Top*) The local field potential (LFP) for each trial was simulated by convolving the spike train with a negative Gaussian with a standard deviation of 2 ms (*blue trace*). (*Bottom*) The spike times were first shifted randomly from a uniform distribution between [–5 5] ms and then convolved with the negative Gaussian to yield the LFP (*orange trace*). (*b*) Average power spectral density across trials of the simulated LFPs, computed between 250 and 750 ms duration, using the multitaper method with a single taper (Bokil et al. 2010). Different traces show different amounts of spike jitter, as indicated in the legend. (*c*) Spike-triggered LFP average, computed by taking a ±20-ms LFP segment around each spike and averaging these segments. (*d*) Spike–field coherence, computed using the multitaper method with a single taper (Bokil et al. 2010). (*e–h*) As in panels *a–d*, but after adding 1-s segments of LFP data (recorded from area V1 of awake monkeys when no stimulus was presented) to the simulated LFPs. The dotted orange trace in panel *f* is the same as the orange trace in panel *b* to show that real LFP power below approximately 50 Hz far exceeds the power of the spike-related transient. Note that the low-frequency component of the LFP that is not phase-locked to the spikes, although it reduces the spike–field coherence at low frequencies, does not appreciably change the spike-triggered LFP average.

2008). Furthermore, this spike-related transient is difficult to detect when correlation is weak (**Figure 2*c*,*g***), although it still has a substantial effect on the SFC (**Figure 2*d*,*b***). Some studies have partially addressed this issue by cutting out the spike-related transient by subtracting the mean waveform before low-pass filtering (Pesaran et al. 2002), interpolating the LFP in a predefined interval around the spike (Galindo-Leon & Liu 2010), or using a Bayesian framework to estimate the low-frequency LFP that is free of spike-related transient (Zanos et al. 2011). However, these methods require predefined interval ranges to work properly, which may change as the correlation changes (**Figure 2*c*,*g***). Algorithms such as matching pursuit that use sharp Gaussians of varying standard deviations as basis functions to represent spike-related transients have been used (Ray et al. 2008), but these algorithms use a greedy approach that may not completely eliminate the spike-related transient when the underlying rhythm is weak (Ray 2015).

This simulation illustrates an important issue: Even though the underlying phenomenon has no genuine rhythmicity, the gamma frequency range could be a more privileged band compared to nongamma frequencies in observing spike–LFP interactions simply because of the action of the 1/f noise at lower frequencies and higher sensitivity toward small time shifts at higher frequencies. Consequently, a change in the shape, magnitude, or latency of the spike-related transient could be more prominently reflected in the gamma range than in other frequency ranges. For example, changes in correlation in the neuronal population due to sensory stimulation (Churchland et al. 2010) or attention (Cohen & Kohn 2011, Cohen & Maunsell 2009) could cause spurious changes in SFC in the gamma range even in the absence of any genuine gamma rhythmicity. Similarly, interactions between two neural assemblies, which could affect the latency and shape of the spike-related transient, could be partially read out by studying the spike–LFP phase relationship (Besserve et al. 2015).

In addition to the spike-related transient in the LFP that is associated with each spike, there are other stereotypical fluctuations in the LFP that are associated with an increase in spiking activity. For example, the onset of a stimulus increases firing rate but also produces a dip in the LFP signal that extends to 100–200 ms (for example, see Ray & Maunsell 2010, figure 1*a*,*d*,*g*). In the frequency domain, such stereotypical fluctuations correspond to low frequencies in the delta or theta range. This observation is important when studying LFP responses for stimuli such as natural images or movies, which do not generally produce salient gamma oscillations (Bartoli et al. 2019, 2020; Hermes et al. 2015; Kanth & Ray 2020; Kayser et al. 2003) unless the RF contains a grating-like feature or long-wavelength hues (Brunet et al. 2013, Kanth & Ray 2020). For example, Rasch and colleagues (2008) recorded from area V1 of anesthetized and nonanesthetized monkeys while showing commercial movie clips and used the high-frequency content of the signal to extract multi-unit activity (MUA). They found a sharp spike-related transient (Rasch et al. 2008, figure 2*a*) followed by a low-frequency upswing, which has been shown to be due to the action of the high-pass filter (Okun 2017) (filtering-related issues are discussed in more detail below). They also found clustering of spikes near large negative fluctuations in the LFP (Rasch et al. 2008, figure 3), likely due to sudden changes in stimulus properties in movie scenes. Therefore, the low-frequency spike–LFP phase relationship conveyed information about the natural images (Montemurro et al. 2008), as did high-frequency LFP activity in the gamma band (Belitski et al. 2008, Rasch et al. 2008).

To summarize, the spike–gamma phase relationship could convey important information about sensory processing and behavior, even in the absence of any rhythmicity in the gamma range in the LFP. While these analyses are important to understand the way neural assemblies process information, care should be taken to distinguish these from the effect of genuine gamma oscillations that are generated due to the action of specific inhibitory mechanisms (as discussed below) and are visible as a prominent narrowband bump in the PSD of the LFP.

GENERATION OF GAMMA RHYTHM

To understand phase locking of spikes with the gamma rhythm observed in the LFP, it is important to understand both how gamma rhythms are generated and how these mechanisms are reflected in the LFP. The generation of gamma rhythms has been extensively studied, both experimentally and using models. While there are several different mechanisms and involvement of different classes of interneurons (Cardin 2016), the best-studied mechanism involves an inhibitory (I) network consisting of parvalbumin-positive, soma-targeting interneurons that provides rhythmic inhibition to the excitatory (E) pyramidal cells, with the rhythm sustained either exclusively by the inhibitory population [I–I or interneuron network gamma (ING) models] or with interaction with pyramidal cells [E–I or pyramidal–interneuron network gamma (PING) models] (Bartos et al. 2007, Börgers & Kopell 2008, Buzsáki & Wang 2012, Tiesinga & Sejnowski 2009, Wang 2010, Whittington et al. 2000). While there are some situations in which the I population may fire before the E population [for example, the phase walkthrough described by Börgers & Kopell (2005)], the most common scenario is that the I population requires excitation from the E population to fire, the resulting inhibition shuts out the entire circuitry, and the cycle repeats when the E population recovers from the inhibition and fires again. In this model, the E cells fire first (only a subset may participate in each gamma cycle), and the I cells follow after a few milliseconds. Such a relationship has been observed in several species, including rodents (Csicsvari et al. 2003), ferrets (Hasenstaub et al. 2005), and monkeys (Vinck et al. 2013).

The default E–I interaction described above could be one mechanism to maintain E–I balance (Haider et al. 2006, Shu et al. 2003); in this interaction, excitatory and inhibitory inputs change proportionally to balance each other, with inhibition lagging excitation by 3–4 ms (Okun & Lampl 2008, Wehr & Zador 2003). Such E–I balance has been linked to a variety of neural processes such as modulation of neuronal selectivity (Isaacson & Scanziani 2011, Wehr & Zador 2003) and gain (Chance et al. 2002, Haider & McCormick 2009), selective gating (Bhatia et al. 2019, Vogels & Abbott 2009), and efficient coding (Denève & Machens 2016, Zhou & Yu 2018). In this case, gamma oscillations are a byproduct of this E–I balance mechanism, with its instantaneous center frequency and amplitude dependent on the instantaneous excitatory and inhibitory conductance (Atallah & Scanziani 2009, Veit et al. 2017). Below, I discuss other hypotheses involving gamma oscillations relative to this default hypothesis.

How is the E and I population firing reflected in the LFP? LFPs are thought to reflect the summed transmembrane currents flowing through the neurons around the microelectrode (Buzsáki et al. 2012, Einevoll et al. 2013). The transmembrane current has a capacitive part that is proportional to the first derivative of the membrane potential and an ionic part that is directly proportional to the membrane potential (Henze et al. 2000). Although the total transmembrane current flowing through a cell is negligible, separation between the inward (sink) and outward (source) transmembrane currents leads to a dipole or a higher-order pole, which generates a measurable potential outside of the cell (Buzsáki et al. 2012, Einevoll et al. 2013). The currents flowing through the pyramidal cells are thought to dominate the LFP, since they are larger than interneurons, and a large fraction of them are aligned perpendicular to the cortical layers, leading to larger dipoles that are well aligned (Einevoll et al. 2013, Mazzoni et al. 2015, Pesaran et al. 2018).

Mazzoni and colleagues (2015) studied several proxies of the LFP using a leaky integrate-and-fire (LIF) model. They obtained several outputs of the LIF network, such as firing rates, membrane potentials, and synaptic currents of both excitatory and inhibitory neurons and tested which output (or their combination) best represented the ground-truth LFP that they obtained by injecting the synaptic input currents of the LIF network into a detailed biophysical network model with realistic morphology. They found that the sum of absolute values of synaptic currents (with

both excitatory and inhibitory currents weighted nearly equally) served as the best proxy for the LFP. This is paradoxical because the two types of synaptic currents are of opposite signs and yet contribute to the LFP with the same sign. This is because the LFP depends on the location of the current sinks and sources relative to the position of the electrode. In particular, the parvalbumin-positive interneurons are soma targeting (Bartos et al. 2007, Buzsáki & Wang 2012, Hu et al. 2014), while the excitatory synapses are distributed over the whole surface of pyramidal neurons. Thus, somatic inhibitory currents can be equivalent to excitatory currents at the apical dendrites. When each proxy was tested alone, the inhibitory currents outperformed other proxies. Mazzoni and colleagues (2015) also showed a 180° phase reversal in the LFP signal near the granular layer, which is also observed in laminar recordings (Kajikawa & Schroeder 2011). In the superficial or granular layers, which are usually sampled with chronic array recordings (Das & Ray 2018, Jia et al. 2013b) and where gamma rhythms are most prominent (Buffalo et al. 2011, Xing et al. 2012b), the synaptic currents (both excitatory and inhibitory) produce a downward deflection or a trough in the LFP signal. Therefore, we expect the excitatory cells to fire a few milliseconds before the gamma trough in the LFP, with the inhibitory cells lagging by a few milliseconds and firing nearer the gamma trough, as has been found experimentally (e.g., Hasenstaub et al. 2005). This phase relationship, however, may be dependent on the recording layer (Welle & Contreras 2016), as well as the type of neurons (Hasenstaub et al. 2016).

SPIKES TEND TO OCCUR NEAR THE TROUGH OF THE GAMMA RHYTHM IN THE LOCAL FIELD POTENTIAL

In this section, I discuss the spike–gamma phase relationship observed in the visual cortex at both gamma and nongamma frequencies. Because of the spike-related transient, which can be decomposed as a series of sinusoids with their troughs aligned to the spike, the spike–LFP phase angle is trivially around 180° (where 0° is considered the peak of the rhythm) at all frequencies when there is no genuine rhythm in the LFP. This is shown in a representative data set (**Figure 3**) where spikes and LFP were recorded from the primary visual cortex (area V1) of monkeys while they attended to a Gabor stimulus of varying contrast (Das & Ray 2018, Ray & Maunsell 2010). These stimuli produce strong gamma oscillations, whose center frequency increases with contrast (**Figure 3*a***; for more details, see Ray & Maunsell 2010). In area V1, attention increases the center frequency of gamma but reduces the magnitude and coherence (Chalk et al. 2010, Das & Ray 2018), unlike in higher visual areas such as area V4, where attention increases field–field, spike–field, and spike–spike coherence (Fries et al. 2008). Although the gamma rhythm was localized to a narrow frequency range, the spike–LFP phase (**Figure 3*b***) was approximately 180° at very low frequencies and slowly increased with frequency. When spikes and LFPs were recorded from the same electrode, the SFC was higher at all frequencies, and the phase remained closer to 180°, compared to when spikes and LFPs were recorded from different electrodes. This is because, when using the same electrode, the spike-related transient is much stronger, which tends to pull the phase toward 180°. The circular standard deviation (Berens 2009), which varies between 0 and $\sqrt{2}$, showed a distinct reduction in the gamma range, suggesting that the rhythm indeed enhanced phase-locking with spikes (**Figure 3*c***), although the standard deviation was substantial, and the preferred phase in the gamma range followed the same trend as nongamma frequencies (**Figure 3*b***). The standard deviation was lower when spikes and LFPs were taken from the same electrode, again due to a larger spike-related transient.

The slow increase in phase with increasing frequency is at least in part due to hardware filters that are used to low-pass filter the raw signal to get the LFP, which is an essential step before sampling to prevent aliasing. Since these are causal filters, they produce a nonzero delay in the

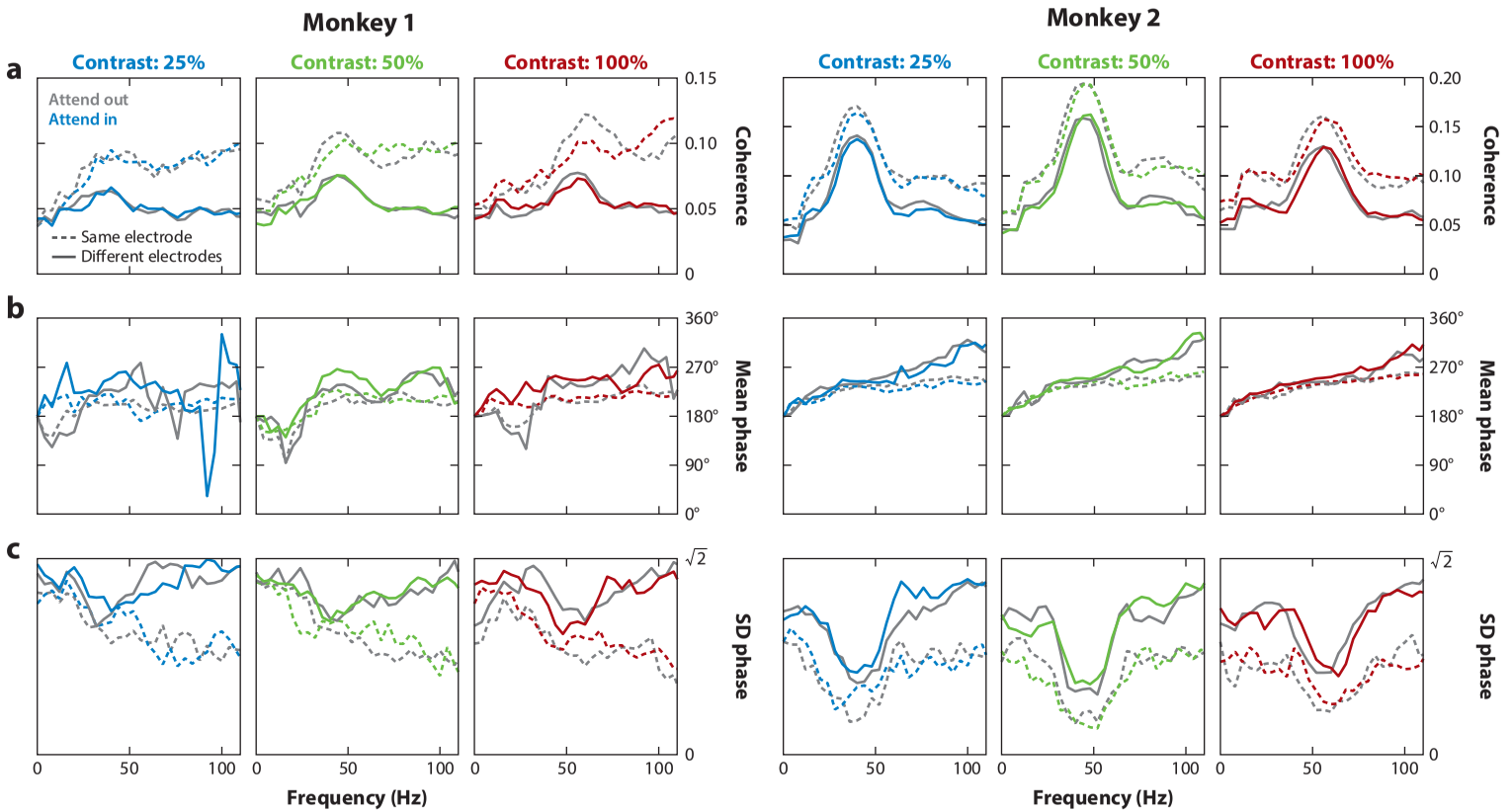

Figure 3

Spike–LFP phase relationship for different stimulus and attentional conditions. (*a*) Column 1 shows the average spike–field coherence computed using spikes and local field potentials (LFPs) from the same electrode ($N = 23$; *dotted lines*) or different electrodes ($N = 163$; *solid lines*) recorded from area V1 of a monkey, when the animal was either paying attention to a Gabor stimulus of 25% contrast inside the receptive field (*colored traces*) or focused away from the stimulus (*gray traces*). Columns 2 and 3 show the same plots for stimuli of 50% and 100% contrasts, respectively, while Columns 4–6 show the same results from another monkey with 39 same and 170 different spike–LFP electrode pairs. Panel adapted from Das & Ray (2018) (CC BY 4.0). (*b*) Circular mean phase for the conditions described in panel *a*. By convention, 180° means that spikes occur at the trough of the LFP, and phase values greater than 180° correspond to spike occurrences before the LFP trough. (*c*) Circular standard deviation (SD) for the conditions described in panel *a*. This measure varies between 0 (complete phase consistency) and $\sqrt{2}$ (completely random phase distribution). Note the reduction in SD in the gamma range and the smaller SD values when spikes and LFPs are recorded from the same electrode.

signal. In general, different frequency components may get shifted by different durations (called the group delay, which is a function of frequency), leading to a distortion of the signal. The Blackrock system used for this recording uses Butterworth filters for low-pass filtering; these filters have a group delay that is constant over a large frequency range to minimize distortion, but their use leads to a linear phase shift, as seen in **Figure 3*b***. A high-pass filter that is often used to filter out the slow drifts in raw signals also produces strong artifacts in the LFP, in particular a large positive peak lasting several hundred milliseconds in the spike-triggered LFP (Okun 2017). However, the phase shift in the data is not fully accounted for by the filtering artifact. For example, the spike–LFP phase in the gamma range was approximately 240° (when using different electrodes for spikes and LFP), which reduced to approximately 230° when filtering-related shifts were accounted for (Das & Ray 2018). This approximately 50° shift from 180° for an oscillation at approximately 45 Hz suggests that spikes preferentially occurred (1,000/45) × (50/360) or approximately 3.1 ms before the gamma trough. It is important to note that in these chronic recordings, the isolation quality is often poor, and most spikes were actually MUA. Furthermore, it was not possible to determine whether spikes were generated by E or I cells.

Several studies have reported a similar spike–gamma phase relationship when using stimuli designed to produce strong gamma oscillations. The earliest microelectrode recordings of gamma oscillations in cats reported the occurrence of spikes near the trough of the rhythm (Eckhorn et al. 1988, Gray & Singer 1989, Gray et al. 1992), although some spike-triggered LFP traces show a shift of 4–5 ms from the trough (for example, see Gray & Singer 1989, figure 2*d*). Chalk and colleagues (2010), using tungsten-in-glass microelectrodes to record both spikes and LFP, showed a spike–LFP phase value of -0.65π or –117° (equivalently, 243°) between 36 and 48 Hz, or approximately 4 ms preceding the trough. Furthermore, they showed that this phase relationship did not change with contrast or attention. Vinck and colleagues (2010a) showed an average phase of approximately 137° when a preferred orientation was presented, although it changed to approximately 159° for the nonpreferred orientation. They used a convention where a leftward shift of the spike relative to the trough decreased the phase, so these results translate to approximately 223° and approximately 201° per the convention used in this review. However, the shift of approximately 20° between preferred and nonpreferred orientations could simply be due to the reduction in actual gamma power for the nonpreferred orientation, which increases the relative influence of the spike-related transient and pulls the phase toward 180° (Das & Ray 2018). Jia and colleagues (2013a, figure 2*c*) also found clustering of spikes near the gamma trough in V1, although they did not report the exact phase values. Rasch and colleagues (2008, figure 2*c–d*), who used natural movies that did not produce strong gamma oscillations, found a preferred spike–LFP phase of 180° at approximately 10 Hz, which slowly increased with frequency, similar to the results shown in **Figure 3** at nongamma frequencies.

Because many of the above-mentioned studies used MUA, one possibility could be that well-isolated spikes were tightly locked to different phases of the gamma rhythm (Havenith et al. 2011), but this relationship could not be observed when the single units could not be isolated. To address this, Martin & Schröder (2016) recorded well-isolated spikes using three very-high-impedance electrodes and LFP from a lower-impedance electrode from area V1 of an anesthetized cat while presenting a wide variety of stimuli including gratings, movies, and visual noise. They found a strong spike-related transient and a similar phase drift (Martin & Schröder 2016, figure 3; note that in their convention, spikes occurring earlier in the LFP phase had lower phase values). At 50 Hz, the phase was 2 radians, or a shift of $\pi - 2$ or 65°, which translates to 3.6 ms of lag at 50 Hz. The results were similar whether the analysis was done at periods of high or low spiking activity, although the circular standard deviation was lower in the former condition. These results

show that even when well-isolated single units are considered, the spike–LFP phase relationship is similar to the relationship observed with MUA.

These studies are consistent with the classic PING-type network behavior described in the previous section. This mechanism also implies that gamma rhythm in the LFP should have a steep trough, corresponding to the activation of the inhibitory population, and a relatively broad peak. Such a nonsinusoidal gamma shape in the LFP has indeed been observed in several experimental (see Bartoli et al. 2019, figure 2*a*; Brunet et al. 2013, figure 2; Henrie & Shapley 2005, figure 1; Jia & Kohn 2011, figure 2; Jia et al. 2011, figure 1*a*; Krishnakumaran et al. 2022, figure 3; Xing et al. 2012a, figure 2) and theoretical (Mazzoni et al. 2015) studies. Krishnakumaran and colleagues (2022) have recently shown that the gamma shape can be used to constrain the models and their operating parameter space. For example, this shape is inconsistent with a model that considers gamma as filtered noise (Burns et al. 2011, Jia et al. 2013b, Xing et al. 2012a) but consistent with a simple Wilson-Cowan-based model (Wilson & Cowan 1972) operating in an inhibition-stabilized network state (Tsodyks et al. 1997), but only when the inhibitory population operated in a superlinear regime (for details, see Jadi & Sejnowski 2014). The waveform shape also has important implications related to various coding schemes (for a detailed discussion, see Cole & Voytek 2017).

While the preferred phase-locking angle is a few milliseconds before the trough on average, there is considerable variability across sites (Jia et al. 2013a) because the phase-locking is generally weak, as reflected in the low coherence values (**Figure 3*a***) and high standard deviation (**Figure 3*c***). Furthermore, slight differences among the timings are expected depending on the neuron type (excitatory and inhibitory), the recording layer, or the exact mechanism of gamma generation within an E–I balance framework.

SPIKE–GAMMA PHASE RELATIONSHIP UNDER DIFFERENT HYPOTHESES

Binding-by-Synchrony

Gamma oscillations rose to prominence due to a seminal discovery that long continuous bars produce strong and synchronous gamma oscillations in the visual cortex, and this enhanced synchrony between neurons was proposed to bind relevant stimulus features into a coherent representation (for reviews, see Singer 1999, Singer & Gray 1995). These studies showed evidence of zero-lag synchrony (calculated using cross-correlation between spiking activity recorded from different sites) that extended over large distances within an area (up to 7 mm in Area 17 of the cat; see Gray et al. 1989) and across visual areas (Engel et al. 1991b). Zero-lag synchrony was reported even across homologous cortical areas of the two hemispheres, which was abolished when the corpus callosum was resected (Engel et al. 1991a). In studies where LFPs were reported, spikes were found to be near the trough (Eckhorn et al. 1988, Gray & Singer 1989, Gray et al. 1992). These results indicated the presence of synchronization across parts of visual cortex, consistent with binding-by-synchrony (BBS) (Gray 1999, Singer 1999) but inconsistent with proposals such as communication-through-coherence (CTC) (discussed below).

Such a spike–gamma relationship is expected in a scenario where the local gamma networks in each area become synchronized, a process for which some mechanisms have been proposed (Traub et al. 1996). However, while the recruitment of such inhibitory networks may lead to enhanced synchrony in the network, whether this synchrony is used by the brain for computation is a different question. For example, Zandvakili & Kohn (2015) showed that spiking in the input layers of area V2 was preceded by brief epochs of elevated area V1 synchronization, but this did not happen for other layers, suggesting that enhanced synchronization in area V1 does not propagate

across multiple downstream areas; such nonpropagation has also been shown by Schneider and colleagues (2021). This classic debate over temporal versus rate coding schemes has been discussed extensively elsewhere (Ainsworth et al. 2012, Shadlen & Movshon 1999, Singer 1999).

Communication-through-Coherence

In CTC, communication between two areas is facilitated if the two neuronal assemblies oscillate such that their excitabilities are properly aligned, taking into account the conduction delay that determines the optimal phase difference (Fries 2005, 2015). Some models have shown that such gamma-based selection can be implemented in simple E–I networks (Börgers & Kopell 2008, Gielen et al. 2010, Tiesinga & Sejnowski 2010). This hypothesis predicts that when two competing neural (sender) assemblies in one area want to communicate with a downstream (receiver) area, the phase angles between the LFPs in the receiver should be well aligned with only one of the two assemblies. However, spikes in both sender and receiver areas are at the most excitable phase of their local LFPs (near the trough), so the local spike–gamma phase relationship does not change in this scheme.

There is evidence both in favor of and against the CTC hypothesis. In support of this prediction, Womelsdorf and colleagues (2007) computed MUA–MUA and MUA–LFP phase angles and power values across trials, binned trials based on their difference from the mean phase angle (which they termed good phase relation), and showed that the trials for which the phase angles were good had stronger correlation in power compared to trials with bad phase relation. The evidence was indirect, since in three out of four data sets, MUA and LFPs were recorded from the same area. Furthermore, correlations are often difficult to interpret because they are sensitive to the total response strength (Cohen & Kohn 2011). Since gamma occurs in short bursts (see below), trials with weak gamma would have low power and random phase, while trials with stronger gamma would have high power and a more well-defined phase. Trials with proper phase relationships may have higher power on average, potentially leading to higher correlation. Furthermore, since the relationship between correlation and response strength may be nonlinear, it may not be fully accounted for using regression or partialization.

A more direct test of CTC was done in two studies in which simultaneous recordings were made from monkey areas V1 and V4 (Bosman et al. 2012, Grothe et al. 2012). Two small stimuli that activated separate V1 sites but the same V4 recording site were presented, and the monkeys attended to one of the two stimuli. The authors showed that field–field phase coherence between areas V1 and V4 was considerably higher for the V1 site that was attended. Bosman and colleagues (2012) further used Granger causality to show feedforward bottom-up directional influence from the attended (but not the unattended) V1 site to the V4 site in the gamma range.

While these results show interesting interactions between neural assemblies that depend on the attentional state, these interactions do not provide unequivocal evidence in favor of CTC, since the crucial prediction of CTC relates to phase difference, not phase consistency. Specifically, if the unattended V1 site consistently has a poor phase relationship with the V4 site, then communication will be hindered, as per CTC, but the coherence (which is a measure of phase consistency irrespective of the phase difference) will nonetheless be high. The crucial prediction of CTC is that the two V1 sites should have nonzero phase difference with respect to each other, and only the attended V1 site should have phase difference with the V4 site that is consistent with the latency between these two areas. However, these studies did not report phase differences between the unattended versus attended V1 site and the V4 site. These studies also used different referencing schemes [bipolar reference (Bosman et al. 2012) versus average reference or single-electrode reference (Grothe et al. 2012)] to address issues related to volume conduction, but such referencing distorts both coherence and phase angles (Shirhatti et al. 2016).

Recently, Rohenkohl and colleagues (2018) showed that the phase relation between areas V1 and V4 can be used to predict behavior: Trials in which the V1–V4 phase angle was closer to the mean (which they considered good) produced shorter reaction times, but only when the stimulus was attended. Similar alignment of phase angle with attention has also been reported between the frontal eye field and area V4 (Gregoriou et al. 2009). However, in these studies, a single stimulus was presented in the RF, so the key prediction of preferred phase alignment of one (but not the other) sender area and the downstream receiver area cannot be directly tested. Consider the default E–I model described above, in which incoming feedforward excitation from the sender area sets up a local gamma in the receiver area based on its local E–I interactions. In this case as well, the gamma oscillations in sender and receiver areas are expected to show a latency-dependent phase relation, which might further be dependent on the attentional state or behavior. Consistent with this, Schneider and colleagues (2021) have shown that peaks in both coherence and granger causality spectra can arise when spiking activity in a sending area causes postsynaptic potentials both in the sender and in the receiver area, suggesting that coherence is not the cause but rather the consequence of communication. Indeed, changes in coherence can be due to many factors, such as firing rates and power, independent of a change in oscillatory coupling (Schneider et al. 2021, Srinath & Ray 2014). Furthermore, to achieve selective communication, the target and distractor networks must satisfy additional constraints, such as differentiability in amplitude, phase, or frequency of oscillatory modulation (Akam & Kullmann 2012). These studies show that the relationship between communication and coherence is complicated; an increase in coherence does not necessarily translate to enhanced communication.

Jia and colleagues (2013a) tested for evidence of CTC using simultaneous recordings from areas V1 and V2. They showed that large visual stimuli produced stronger gamma oscillations in both areas V1 and V2 compared to smaller stimuli, which led to enhanced pairwise and higher-order synchrony in the neurons in area V1 and produced stronger V1–V2 spike coupling for pairs with retinotopically aligned RFs. However, when they computed the probability of a V2 spike following a V1 spike within the expected delay of approximately 3 ms (estimated using cross-correlation analysis), this probability varied systematically with the preferred phase of gamma in area V1 but not in area V2 (Jia et al. 2013a, figure 7*c* versus figure 7*f*). Therefore, enhanced V1–V2 coupling arose from enhanced temporal coordination of V1 spiking due to the local gamma in area V1, but not when the spikes arrived from area V1 at the optimal window set by V2 gamma, as proposed by the CTC hypothesis.

Gamma Phase-Coding

In gamma phase-coding, sensory information is coded in the timing of the spike relative to the phase of an ongoing oscillation. This was first proposed by Buzsaki & Chrobak (1995) in the framework of inhibitory networks, based on the finding that the position of spikes relative to theta oscillations in the hippocampus of rats carried information about the position of the rat in the environment (O'Keefe & Recce 1993). Similarly, the low-frequency LFP phase was found to carry information about the visual stimulus (Montemurro et al. 2008). This concept was later extended for gamma oscillations by Fries and colleagues (2007). In their work, a neuron receiving a stronger stimulus is expected to overcome the inhibition earlier and fire earlier in the gamma cycle compared to neurons receiving weaker stimuli, for which the neuron can only fire near the trough of the rhythm, when inhibition is lowest. As discussed above, phase difference consistent with this hypothesis has been shown by Vinck and colleagues (2010a), but phase estimates are likely to be confounded by the differences in absolute gamma power or firing rates among different conditions. Several other studies (as discussed above) have either failed to observe any phase shift with stimulus intensity or attention (Chalk et al. 2010) or been able to account for

the phase differences based on changes in oscillation frequency across conditions (Das & Ray 2018).

Gain Modulation, Selection, and Multiplexing

A variety of (often interrelated) proposals have been made in which gamma oscillations arising out of E–I interactions modulate the gain of the cortical area (Azouz & Gray 2003, Ni et al. 2016, Tiesinga et al. 2004), allow a subset of inputs to be selected at the expense of others (Akam & Kullmann 2010, Börgers & Kopell 2008, Gielen et al. 2010), or allow multiplexing of multiple inputs at different frequencies (Akam & Kullmann 2014). Unlike BBS and CTC, these proposals involve the action of gamma within an area (Sohal 2016). As discussed below, many of these mechanisms involve basic E–I interactions (Ferguson & Cardin 2020) and can be equivalently framed in a pro- or antirole fashion, especially when the rhythm itself is of brief duration.

BURSTY NATURE OF GAMMA OSCILLATIONS

In discussions of a potential role of gamma rhythm in cortical processing, an important factor is the duration of the rhythm. Previous studies have shown that gamma rhythm in the primary visual cortex occurs in short bursts of 100–200 ms duration (Rols et al. 2001, Xing et al. 2012a) and is best characterized as filtered noise in which bursts simply reflect stochastic fluctuations in amplitude (Burns et al. 2010, 2011). Such burstiness has also been observed in other rhythms (Jones 2016, van Ede et al. 2018), such as the beta rhythm in the striatum and premotor–motor cortex (Feingold et al. 2015) and prefrontal cortex (Lundqvist et al. 2016), in multiple species, as well as in models (Sherman et al. 2016). Chandran KS and colleagues (2017) recently showed that the apparent burstiness could arise due to the variability in spectral estimators, even when the rhythm itself is not bursty. By using a matching pursuit–based algorithm (Chandran KS et al. 2016, Mallat & Zhang 1993) that allowed estimation of burst duration in the time domain itself, Chandran KS and colleagues (2016) showed that the median duration of gamma rhythm was approximately 300 ms. However, the distribution of gamma bursts (see Chandran KS et al. 2017, figure 7*b*) still revealed a clear mode at approximately 100 ms with a heavy tail, suggesting that gamma tends to mainly appear in short bursts with occasional longer bouts.

Recent models have shown that even though gamma oscillations are bursty, and the instantaneous frequency varies considerably, transient epochs of matched frequencies and timing can be used for flexible routing (Palmigiano et al. 2017). Lowet and colleagues (2017) also showed that maintenance of phase relations and synchronization required modulations in instantaneous frequencies and explained these interactions using weakly coupled oscillators. However, the short duration of gamma rhythm makes any debate about a functional role largely a matter of semantics. As described above, the physiological phenomenon is the activation of an inhibitory network recruited by the incoming excitation, which subsequently modulates the excitability of the pyramidal neurons. A prorole description of this phenomenon would state that the recruitment of inhibitory neurons generates a transient gamma rhythm, which generates a few alternating epochs of low and high excitability. An antirole description of the same phenomenon would state that the interneurons hyperpolarize the network, which eventually rebounds back as the inhibition fades away at a rate corresponding to gamma frequencies and is, therefore, an epiphenomenon of the underlying E–I interaction. The question of whether the gamma rhythm plays a role in cortical processing is vague and irrelevant; emphasis should instead be on the physiological mechanisms (Doelling & Assaneo 2021).

Most of the proposed hypotheses do not require long epochs of gamma. Sensory information in the visual cortex moves rapidly such that onset latencies between one area and the immediately

downstream area are on the order of a single gamma cycle (approximately 20 ms), with considerable variation in latencies within each area (Schmolesky et al. 1998). For example, Schmolesky and colleagues reported latencies in areas V1, V2, and V4 (mean ± standard deviation) of 66 ± 10.7, 82 ± 21.1, and 104 ± 23.4 milliseconds, respectively. Sensory excitation and resulting feedback inhibition within each area would cause at least one cycle of gamma rhythm in each area (whether to consider this as a rhythm is subjective), and such transient gamma bursts across areas will have some latency-dependent phase relationship. One interesting question is, since the typical duration of gamma is >100 ms (at least four cycles), are the subsequent cycles of gamma of any relevance, or are they mere reverberations? Unfortunately, this question is difficult to address using standard signal processing techniques because of the time–frequency uncertainty principle (Chandran KS et al. 2016, Pesaran et al. 2018). Spectral resolution depends on the time interval over which analysis is done (the so-called Rayleigh frequency is given by 1/T, where T corresponds to the analysis interval; for a more detailed discussion, see Chandran KS et al. 2016). To get a reasonable spectral resolution, stationarity must be assumed over at least 150–200 ms, and the resulting estimate of power or phase consistency is essentially the average over that interval. For example, the SFC evaluated over 200 ms to get a spectral resolution of 5 Hz yields the average phase consistency over approximately eight gamma cycles.

Regardless of whether gamma oscillations play a role in cortical processing, it is clear that they provide a unique signature by which to study E–I interactions that can be observed in noninvasive signals such as electroencephalogram or magnetoencephalogram (Pesaran et al. 2018). These E–I interactions and gamma oscillations are altered in a variety of mental disorders such as autism, schizophrenia, and Alzheimer's disease (Murty et al. 2021; Sohal & Rubenstein 2019; Uhlhaas & Singer 2010, 2012). This, together with the observation that the gamma band may be more privileged to capture signatures of neural processes even when these processes do not involve genuine gamma rhythmicity, makes gamma an important tool to study brain function.

DISCLOSURE STATEMENT

The author is not aware of any affiliations, memberships, funding, or financial holdings that might be perceived as affecting the objectivity of this review.

ACKNOWLEDGMENTS

This work was supported by the Wellcome Trust/DBT India Alliance (IA/S/18/2/504003; senior fellowship) and the DBT-IISc Partnership Program. I thank Stefano Panzeri, Martin Vinck, Aritra Das, and Surya Prakash for valuable comments on this manuscript.

LITERATURE CITED

Ainsworth M, Lee S, Cunningham MO, Traub RD, Kopell NJ, Whittington MA. 2012. Rates and rhythms: a synergistic view of frequency and temporal coding in neuronal networks. *Neuron* 75(4):572–83

Akam TE, Kullmann DM. 2010. Oscillations and filtering networks support flexible routing of information. *Neuron* 67(2):308–20

Akam TE, Kullmann DM. 2012. Efficient "communication through coherence" requires oscillations structured to minimize interference between signals. *PLOS Comput. Biol.* 8(11):e1002760

Akam TE, Kullmann DM. 2014. Oscillatory multiplexing of population codes for selective communication in the mammalian brain. *Nat. Rev. Neurosci.* 15(2):111–22

Atallah BV, Scanziani M. 2009. Instantaneous modulation of gamma oscillation frequency by balancing excitation with inhibition. *Neuron* 62:566–77

Azouz R, Gray CM. 2003. Adaptive coincidence detection and dynamic gain control in visual cortical neurons in vivo. *Neuron* 37(3):513–23

Bartoli E, Bosking W, Chen Y, Li Y, Sheth SA, et al. 2019. Functionally distinct gamma range activity revealed by stimulus tuning in human visual cortex. *Curr. Biol.* 29(20):3345–58.e7
Bartoli E, Bosking W, Foster BL. 2020. Seeing visual gamma oscillations in a new light. *Trends Cogn. Sci.* 24(7):501–3
Bartos M, Vida I, Jonas P. 2007. Synaptic mechanisms of synchronized gamma oscillations in inhibitory interneuron networks. *Nat. Rev. Neurosci.* 8(1):45–56
Belitski A, Gretton A, Magri C, Murayama Y, Montemurro MA, et al. 2008. Low-frequency local field potentials and spikes in primary visual cortex convey independent visual information. *J. Neurosci.* 28:5696–709
Berens P. 2009. CircStat: a MATLAB toolbox for circular statistics. *J. Stat. Softw.* 31:i10
Berens P, Keliris GA, Ecker AS, Logothetis NK, Tolias AS. 2008. Comparing the feature selectivity of the gamma-band of the local field potential and the underlying spiking activity in primate visual cortex. *Front. Syst. Neurosci.* 2:2
Besserve M, Lowe SC, Logothetis NK, Schölkopf B, Panzeri S. 2015. Shifts of gamma phase across primary visual cortical sites reflect dynamic stimulus-modulated information transfer. *PLOS Biol.* 13(9):e1002257
Bhatia A, Moza S, Bhalla US. 2019. Precise excitation-inhibition balance controls gain and timing in the hippocampus. *eLife* 8:e43415
Bokil H, Andrews P, Kulkarni JE, Mehta S, Mitra PP. 2010. Chronux: a platform for analyzing neural signals. *J. Neurosci. Methods* 192(1):146–51
Börgers C, Kopell N. 2005. Effects of noisy drive on rhythms in networks of excitatory and inhibitory neurons. *Neural Comput.* 17(3):557–608
Börgers C, Kopell NJ. 2008. Gamma oscillations and stimulus selection. *Neural Comput.* 20(2):383–414
Bosman CA, Schoffelen J-M, Brunet N, Oostenveld R, Bastos AM, et al. 2012. Attentional stimulus selection through selective synchronization between monkey visual areas. *Neuron* 75(5):875–88
Brunet N, Bosman CA, Roberts M, Oostenveld R, Womelsdorf T, et al. 2013. Visual cortical gamma-band activity during free viewing of natural images. *Cereb. Cortex* 25(4):918–26
Buffalo EA, Fries P, Landman R, Buschman TJ, Desimone R. 2011. Laminar differences in gamma and alpha coherence in the ventral stream. *PNAS* 108(27):11262–67
Burns SP, Xing D, Shapley RM. 2011. Is gamma-band activity in the local field potential of V1 cortex a "clock" or filtered noise? *J. Neurosci.* 31(26):9658–64
Burns SP, Xing D, Shelley MJ, Shapley RM. 2010. Searching for autocoherence in the cortical network with a time-frequency analysis of the local field potential. *J. Neurosci.* 30(11):4033–47
Buzsáki G, Anastassiou CA, Koch C. 2012. The origin of extracellular fields and currents—EEG, ECoG, LFP and spikes. *Nat. Rev. Neurosci.* 13(6):407–20
Buzsáki G, Chrobak JJ. 1995. Temporal structure in spatially organized neuronal ensembles: a role for interneuronal networks. *Curr. Opin. Neurobiol.* 5:504–10
Buzsáki G, Wang X-J. 2012. Mechanisms of gamma oscillations. *Annu. Rev. Neurosci.* 35:203–25
Cardin JA. 2016. Snapshots of the brain in action: local circuit operations through the lens of γ oscillations. *J. Neurosci.* 36(41):10496–504
Chalk M, Herrero JL, Gieselmann MA, Delicato LS, Gotthardt S, Thiele A. 2010. Attention reduces stimulus-driven gamma frequency oscillations and spike field coherence in V1. *Neuron* 66(1):114–25
Chance FS, Abbott LF, Reyes AD. 2002. Gain modulation from background synaptic input. *Neuron* 35:773–82
Chandran KS S, Mishra A, Shirhatti V, Ray S. 2016. Comparison of matching pursuit algorithm with other signal processing techniques for computation of the time-frequency power spectrum of brain signals. *J. Neurosci.* 36(12):3399–408
Chandran KS S, Seelamantula CS, Ray S. 2017. Duration analysis using matching pursuit algorithm reveals longer bouts of gamma rhythm. *J. Neurophysiol.* 119(3):808–21
Churchland MM, Yu BM, Cunningham JP, Sugrue LP, Cohen MR, et al. 2010. Stimulus onset quenches neural variability: a widespread cortical phenomenon. *Nat. Neurosci.* 13(3):369–78
Cohen MR, Kohn A. 2011. Measuring and interpreting neuronal correlations. *Nat. Neurosci.* 14(7):811–19
Cohen MR, Maunsell JH. 2009. Attention improves performance primarily by reducing interneuronal correlations. *Nat. Neurosci.* 12:1594–600
Cole SR, Voytek B. 2017. Brain oscillations and the importance of waveform shape. *Trends Cogn. Sci.* 21(2):137–49

Csicsvari J, Henze DA, Jamieson B, Harris KD, Sirota A, et al. 2003. Massively parallel recording of unit and local field potentials with silicon-based electrodes. *J. Neurophysiol.* 90(2):1314–23
Das A, Ray S. 2018. Effect of stimulus contrast and visual attention on spike-gamma phase relationship in macaque primary visual cortex. *Front. Comput. Neurosci.* 12:66
Denève S, Machens CK. 2016. Efficient codes and balanced networks. *Nat. Neurosci.* 19(3):375–82
Doelling KB, Assaneo MF. 2021. Neural oscillations are a start toward understanding brain activity rather than the end. *PLOS Biol.* 19(5):e3001234
Eckhorn R, Bauer R, Jordan W, Brosch M, Kruse W, et al. 1988. Coherent oscillations: a mechanism of feature linking in the visual cortex? Multiple electrode and correlation analyses in the cat. *Biol. Cybern.* 60(2):121–30
Einevoll GT, Kayser C, Logothetis NK, Panzeri S. 2013. Modelling and analysis of local field potentials for studying the function of cortical circuits. *Nat. Rev. Neurosci.* 14(11):770–85
Engel AK, Konig P, Kreiter A, Singer W. 1991a. Interhemispheric synchronization of oscillatory neuronal responses in cat visual cortex. *Science* 252(5009):1177–79
Engel AK, Kreiter AK, König P, Singer W. 1991b. Synchronization of oscillatory neuronal responses between striate and extrastriate visual cortical areas of the cat. *PNAS* 88(14):6048–52
Feingold J, Gibson DJ, DePasquale B, Graybiel AM. 2015. Bursts of beta oscillation differentiate postperformance activity in the striatum and motor cortex of monkeys performing movement tasks. *PNAS* 112(44):13687–92
Ferguson KA, Cardin JA. 2020. Mechanisms underlying gain modulation in the cortex. *Nat. Rev. Neurosci.* 21(2):80–92
Friedman-Hill S, Maldonado PE, Gray CM. 2000. Dynamics of striate cortical activity in the alert macaque: I. Incidence and stimulus-dependence of gamma-band neuronal oscillations. *Cereb. Cortex* 10:1105–16
Fries P. 2005. A mechanism for cognitive dynamics: neuronal communication through neuronal coherence. *Trends Cogn. Sci.* 9(10):474–80
Fries P. 2009. Neuronal gamma-band synchronization as a fundamental process in cortical computation. *Annu. Rev. Neurosci.* 32:209–24
Fries P. 2015. Rhythms for cognition: communication through coherence. *Neuron* 88(1):220–35
Fries P, Nikolić D, Singer W. 2007. The gamma cycle. *Trends Neurosci.* 30(7):309–16
Fries P, Reynolds JH, Rorie AE, Desimone R. 2001. Modulation of oscillatory neuronal synchronization by selective visual attention. *Science* 291:1560–63
Fries P, Womelsdorf T, Oostenveld R, Desimone R. 2008. The effects of visual stimulation and selective visual attention on rhythmic neuronal synchronization in macaque area V4. *J. Neurosci.* 28(18):4823–35
Galindo-Leon EE, Liu RC. 2010. Predicting stimulus-locked single unit spiking from cortical local field potentials. *J. Comput. Neurosci.* 29(3):581–97
Gielen S, Krupa M, Zeitler M. 2010. Gamma oscillations as a mechanism for selective information transmission. *Biol. Cybern.* 103(2):151–65
Gieselmann MA, Thiele A. 2008. Comparison of spatial integration and surround suppression characteristics in spiking activity and the local field potential in macaque V1. *Eur. J. Neurosci.* 28:447–59
Grasse DW, Moxon KA. 2010. Correcting the bias of spike field coherence estimators due to a finite number of spikes. *J. Neurophysiol.* 104(1):548–58
Gray CM. 1999. The temporal correlation hypothesis of visual feature integration: still alive and well. *Neuron* 24(1):31–47, 111–25
Gray CM, Engel AK, König P, Singer W. 1992. Synchronization of oscillatory neuronal responses in cat striate cortex: temporal properties. *Vis. Neurosci.* 8(4):337–47
Gray CM, König P, Engel AK, Singer W. 1989. Oscillatory responses in cat visual cortex exhibit intercolumnar synchronization which reflects global stimulus properties. *Nature* 338(6213):334–37
Gray CM, Singer W. 1989. Stimulus-specific neuronal oscillations in orientation columns of cat visual cortex. *PNAS* 86(5):1698–702
Gregoriou GG, Gotts SJ, Zhou H, Desimone R. 2009. High-frequency, long-range coupling between prefrontal and visual cortex during attention. *Science* 324:1207–10
Grothe I, Neitzel SD, Mandon S, Kreiter AK. 2012. Switching neuronal inputs by differential modulations of gamma-band phase-coherence. *J. Neurosci.* 32(46):16172–80

Hadjipapas A, Adjamian P, Swettenham JB, Holliday IE, Barnes GR. 2007. Stimuli of varying spatial scale induce gamma activity with distinct temporal characteristics in human visual cortex. *NeuroImage* 35:518–30

Haider B, Duque A, Hasenstaub AR, McCormick DA. 2006. Neocortical network activity in vivo is generated through a dynamic balance of excitation and inhibition. *J. Neurosci.* 26:4535–45

Haider B, McCormick DA. 2009. Rapid neocortical dynamics: cellular and network mechanisms. *Neuron* 62(2):171–89

Hasenstaub A, Otte S, Callaway E. 2016. Cell type-specific control of spike timing by gamma-band oscillatory inhibition. *Cereb. Cortex* 26(2):797–806

Hasenstaub A, Shu Y, Haider B, Kraushaar U, Duque A, McCormick DA. 2005. Inhibitory postsynaptic potentials carry synchronized frequency information in active cortical networks. *Neuron* 47:423–35

Havenith MN, Yu S, Biederlack J, Chen N-H, Singer W, Nikolić D. 2011. Synchrony makes neurons fire in sequence, and stimulus properties determine who is ahead. *J. Neurosci.* 31(23):8570–84

Henrie JA, Shapley R. 2005. LFP power spectra in V1 cortex: the graded effect of stimulus contrast. *J. Neurophysiol.* 94:479–90

Henze DA, Borhegyi Z, Csicsvari J, Mamiya A, Harris KD, Buzsáki G. 2000. Intracellular features predicted by extracellular recordings in the hippocampus in vivo. *J. Neurophysiol.* 84(1):390–400

Hermes D, Miller KJ, Wandell BA, Winawer J. 2015. Stimulus dependence of gamma oscillations in human visual cortex. *Cereb. Cortex* 25(9):2951–59

Hu H, Gan J, Jonas P. 2014. Fast-spiking, parvalbumin^{+} GABAergic interneurons: from cellular design to microcircuit function. *Science* 345(6196):1255263

Isaacson JS, Scanziani M. 2011. How inhibition shapes cortical activity. *Neuron* 72(2):231–43

Jadi MP, Sejnowski TJ. 2014. Regulating cortical oscillations in an inhibition-stabilized network. *Proc. IEEE* 102(5):830–42

Jia X, Kohn A. 2011. Gamma rhythms in the brain. *PLOS Biol*. 9(4):e1001045

Jia X, Smith MA, Kohn A. 2011. Stimulus selectivity and spatial coherence of gamma components of the local field potential. *J. Neurosci.* 31(25):9390–403

Jia X, Tanabe S, Kohn A. 2013a. Gamma and the coordination of spiking activity in early visual cortex. *Neuron* 77(4):762–74

Jia X, Xing D, Kohn A. 2013b. No consistent relationship between gamma power and peak frequency in macaque primary visual cortex. *J. Neurosci.* 33(1):17–25

Jones SR. 2016. When brain rhythms aren't "rhythmic": implication for their mechanisms and meaning. *Curr. Opin. Neurobiol.* 40:72–80

Kajikawa Y, Schroeder CE. 2011. How local is the local field potential? *Neuron* 72(5):847–58

Kanth ST, Ray S. 2020. Electrocorticogram (ECoG) is highly informative in primate visual cortex. *J. Neurosci.* 40(12):2430–44

Kayser C, Salazar RF, Konig P. 2003. Responses to natural scenes in cat V1. *J. Neurophysiol.* 90(3):1910–20

Krishnakumaran R, Raees M, Ray S. 2022. Shape analysis of gamma rhythm supports a superlinear inhibitory regime in an inhibition-stabilized network. *PLOS Comput. Biol.* 18(2):e1009886

Li Z, Cui D, Li X. 2016. Unbiased and robust quantification of synchronization between spikes and local field potential. *J. Neurosci. Methods* 269:33–38

Lowet E, Roberts MJ, Bonizzi P, Karel J, De Weerd P. 2016. Quantifying neural oscillatory synchronization: a comparison between spectral coherence and phase-locking value approaches. *PLOS ONE* 11(1):e0146443

Lowet E, Roberts MJ, Gips B, De Weerd P, Peter A. 2017. A quantitative theory of gamma synchronization in macaque V1. *eLife* 6:e26642

Lundqvist M, Rose J, Herman P, Brincat SL, Buschman TJ, Miller EK. 2016. Gamma and beta bursts underlie working memory. *Neuron* 90(1):152–64

Mallat SG, Zhang Z. 1993. Matching pursuits with time-frequency dictionaries. *IEEE Trans. Signal Process.* 41:3397–415

Martin KAC, Schröder S. 2016. Phase locking of multiple single neurons to the local field potential in cat V1. *J. Neurosci.* 36(8):2494–502

Mayo JP, Maunsell JHR. 2016. Graded neuronal modulations related to visual spatial attention. *J. Neurosci.* 36(19):5353–61

Mazzoni A, Lindén H, Cuntz H, Lansner A, Panzeri S, Einevoll GT. 2015. Computing the local field potential (LFP) from integrate-and-fire network models. *PLOS Comput. Biol.* 11(12):e1004584

Mitra PP, Pesaran B. 1999. Analysis of dynamic brain imaging data. *Biophys. J.* 76:691–708

Mitzdorf U. 1985. Current source-density method and application in cat cerebral cortex: investigation of evoked potentials and EEG phenomena. *Physiol. Rev.* 65:37–100

Montemurro MA, Rasch MJ, Murayama Y, Logothetis NK, Panzeri S. 2008. Phase-of-firing coding of natural visual stimuli in primary visual cortex. *Curr. Biol.* 18:375–80

Murty DV, Manikandan K, Kumar WS, Ramesh RG, Purokayastha S, et al. 2021. Stimulus-induced gamma rhythms are weaker in human elderly with mild cognitive impairment and Alzheimer's disease. *eLife* 10:e61666

Murty DVPS, Shirhatti V, Ravishankar P, Ray S. 2018. Large visual stimuli induce two distinct gamma oscillations in primate visual cortex. *J. Neurosci.* 38(11):2730–44

Ni J, Wunderle T, Lewis CM, Desimone R, Diester I, Fries P. 2016. Gamma-rhythmic gain modulation. *Neuron* 92(1):240–51

O'Keefe J, Recce ML. 1993. Phase relationship between hippocampal place units and the EEG theta rhythm. *Hippocampus* 3(3):317–30

Okun M. 2017. Artefactual origin of biphasic cortical spike-LFP correlation. *J. Comput. Neurosci.* 42(1):31–35

Okun M, Lampl I. 2008. Instantaneous correlation of excitation and inhibition during ongoing and sensory-evoked activities. *Nat. Neurosci.* 11(5):535–37

Okun M, Naim A, Lampl I. 2010. The subthreshold relation between cortical local field potential and neuronal firing unveiled by intracellular recordings in awake rats. *J. Neurosci.* 30(12):4440–48

Palmigiano A, Geisel T, Wolf F, Battaglia D. 2017. Flexible information routing by transient synchrony. *Nat. Neurosci.* 20(7):1014–22

Pesaran B, Pezaris JS, Sahani M, Mitra PP, Andersen RA. 2002. Temporal structure in neuronal activity during working memory in macaque parietal cortex. *Nat. Neurosci.* 5(8):805–11

Pesaran B, Vinck M, Einevoll GT, Sirota A, Fries P, et al. 2018. Investigating large-scale brain dynamics using field potential recordings: analysis and interpretation. *Nat. Neurosci.* 21(7):903–19

Prakash SS, Das A, Kanth ST, Mayo JP, Ray S. 2021. Decoding of attentional state using high-frequency local field potential is as accurate as using spikes. *Cereb. Cortex* 31(9):4314–28

Rasch MJ, Gretton A, Murayama Y, Maass W, Logothetis NK. 2008. Inferring spike trains from local field potentials. *J. Neurophysiol.* 99:1461–76

Ray S. 2015. Challenges in the quantification and interpretation of spike-LFP relationships. *Curr. Opin. Neurobiol.* 31:111–18

Ray S, Hsiao SS, Crone NE, Franaszczuk PJ, Niebur E. 2008. Effect of stimulus intensity on the spike-local field potential relationship in the secondary somatosensory cortex. *J. Neurosci.* 28:7334–43

Ray S, Maunsell JHR. 2010. Differences in gamma frequencies across visual cortex restrict their possible use in computation. *Neuron* 67(5):885–96

Ray S, Maunsell JHR. 2011a. Different origins of gamma rhythm and high-gamma activity in macaque visual cortex. *PLOS Biol.* 9(4):e1000610

Ray S, Maunsell JHR. 2011b. Network rhythms influence the relationship between spike-triggered local field potential and functional connectivity. *J. Neurosci.* 31(35):12674–82

Ray S, Maunsell JHR. 2015. Do gamma oscillations play a role in cerebral cortex? *Trends Cogn. Sci.* 19(2):78–85

Rohenkohl G, Bosman CA, Fries P. 2018. Gamma synchronization between V1 and V4 improves behavioral performance. *Neuron* 100(4):953–63.e3

Rols G, Tallon-Baudry C, Girard P, Bertrand O, Bullier J. 2001. Cortical mapping of gamma oscillations in areas V1 and V4 of the macaque monkey. *Vis. Neurosci.* 18:527–40

Schmolesky MT, Wang Y, Hanes DP, Thompson KG, Leutgeb S, et al. 1998. Signal timing across the macaque visual system. *J. Neurophysiol.* 79(6):3272–78

Schneider M, Broggini AC, Dann B, Tzanou A, Uran C, et al. 2021. A mechanism for inter-areal coherence through communication based on connectivity and oscillatory power. *Neuron* 109(24):4050–67.e12

Shadlen MN, Movshon JA. 1999. Synchrony unbound: a critical evaluation of the temporal binding hypothesis. *Neuron* 24(1):67–77, 111–25

Sherman MA, Lee S, Law R, Haegens S, Thorn CA, et al. 2016. Neural mechanisms of transient neocortical beta rhythms: converging evidence from humans, computational modeling, monkeys, and mice. *PNAS* 113(33):E4885–94

Shirhatti V, Borthakur A, Ray S. 2016. Effect of reference scheme on power and phase of the local field potential. *Neural Comput.* 28(5):882–913

Shirhatti V, Ray S. 2018. Long-wavelength (reddish) hues induce unusually large gamma oscillations in the primate primary visual cortex. *PNAS* 115(17):4489–94

Shu Y, Hasenstaub A, McCormick DA. 2003. Turning on and off recurrent balanced cortical activity. *Nature* 423:288–93

Singer W. 1999. Neuronal synchrony: a versatile code for the definition of relations? *Neuron* 24(1):49–65, 111–25

Singer W, Gray CM. 1995. Visual feature integration and the temporal correlation hypothesis. *Annu. Rev. Neurosci.* 18:555–86

Smith MA, Kohn A. 2008. Spatial and temporal scales of neuronal correlation in primary visual cortex. *J. Neurosci.* 28:12591–603

Sohal VS. 2016. How close are we to understanding what (if anything) γ oscillations do in cortical circuits? *J. Neurosci.* 36(41):10489–95

Sohal VS, Rubenstein JLR. 2019. Excitation-inhibition balance as a framework for investigating mechanisms in neuropsychiatric disorders. *Mol. Psychiatry* 24(9):1248–57

Srinath R, Ray S. 2014. Effect of amplitude correlations on coherence in the local field potential. *J. Neurophysiol.* 112(4):741–51

Tiesinga PH, Fellous J-M, Salinas E, Jose JV, Sejnowski TJ. 2004. Inhibitory synchrony as a mechanism for attentional gain modulation. *J. Physiol.* 98:296–314

Tiesinga PH, Sejnowski TJ. 2009. Cortical enlightenment: Are attentional gamma oscillations driven by ING or PING? *Neuron* 63(6):727–32

Tiesinga PH, Sejnowski TJ. 2010. Mechanisms for phase shifting in cortical networks and their role in communication through coherence. *Front. Hum. Neurosci.* 4:196

Traub RD, Whittington MA, Stanford IM, Jefferys JGR. 1996. A mechanism for generation of long-range synchronous fast oscillations in the cortex. *Nature* 383(6601):621–24

Tsodyks MV, Skaggs WE, Sejnowski TJ, McNaughton BL. 1997. Paradoxical effects of external modulation of inhibitory interneurons. *J. Neurosci.* 17(11):4382–88

Uhlhaas PJ, Singer W. 2010. Abnormal neural oscillations and synchrony in schizophrenia. *Nat. Rev. Neurosci.* 11(2):100–13

Uhlhaas PJ, Singer W. 2012. Neuronal dynamics and neuropsychiatric disorders: toward a translational paradigm for dysfunctional large-scale networks. *Neuron* 75(6):963–80

van Ede F, Quinn AJ, Woolrich MW, Nobre AC. 2018. Neural oscillations: sustained rhythms or transient burst-events? *Trends Neurosci.* 41(7):415–17

van Pelt S, Fries P. 2013. Visual stimulus eccentricity affects human gamma peak frequency. *NeuroImage* 78:439–47

Veit J, Hakim R, Jadi MP, Sejnowski TJ, Adesnik H. 2017. Cortical gamma band synchronization through somatostatin interneurons. *Nat. Neurosci.* 20(7):951–59

Vinck M, Battaglia FP, Womelsdorf T, Pennartz C. 2012. Improved measures of phase-coupling between spikes and the local field potential. *J. Comput. Neurosci.* 33(1):53–75

Vinck M, Lima B, Womelsdorf T, Oostenveld R, Singer W, et al. 2010a. Gamma-phase shifting in awake monkey visual cortex. *J. Neurosci.* 30(4):1250–57

Vinck M, van Wingerden M, Womelsdorf T, Fries P, Pennartz CMA. 2010b. The pairwise phase consistency: a bias-free measure of rhythmic neuronal synchronization. *NeuroImage* 51(1):112–22

Vinck M, Womelsdorf T, Buffalo EA, Desimone R, Fries P. 2013. Attentional modulation of cell-class-specific gamma-band synchronization in awake monkey area V4. *Neuron* 80(4):1077–89

Vogels TP, Abbott LF. 2009. Gating multiple signals through detailed balance of excitation and inhibition in spiking networks. *Nat. Neurosci.* 12(4):483–91

Wang X-J. 2010. Neurophysiological and computational principles of cortical rhythms in cognition. *Physiol. Rev.* 90(3):1195–268

Wehr M, Zador AM. 2003. Balanced inhibition underlies tuning and sharpens spike timing in auditory cortex. *Nature* 426(6965):442–46

Welle CG, Contreras D. 2016. Sensory-driven and spontaneous gamma oscillations engage distinct cortical circuitry. *J. Neurophysiol.* 115(4):1821–35

Whittington MA, Traub RD, Kopell N, Ermentrout B, Buhl EH. 2000. Inhibition-based rhythms: experimental and mathematical observations on network dynamics. *Int. J. Psychophysiol.* 38:315–36

Wilson HR, Cowan JD. 1972. Excitatory and inhibitory interactions in localized populations of model neurons. *Biophys. J.* 12(1):1–24

Womelsdorf T, Schoffelen J-M, Oostenveld R, Singer W, Desimone R, et al. 2007. Modulation of neuronal interactions through neuronal synchronization. *Science* 316(5831):1609–12

Xing D, Shen Y, Burns S, Yeh C-I, Shapley R, Li W. 2012a. Stochastic generation of gamma-band activity in primary visual cortex of awake and anesthetized monkeys. *J. Neurosci.* 32(40):13873–80

Xing D, Yeh C-I, Burns S, Shapley RM. 2012b. Laminar analysis of visually evoked activity in the primary visual cortex. *PNAS* 109(34):13871–76

Zandvakili A, Kohn A. 2015. Coordinated neuronal activity enhances corticocortical communication. *Neuron* 87(4):827–39

Zanos TP, Mineault PJ, Pack CC. 2011. Removal of spurious correlations between spikes and local field potentials. *J. Neurophysiol.* 105(1):474–86

Zhou S, Yu Y. 2018. Synaptic E-I balance underlies efficient neural coding. *Front. Neurosci.* 12:46